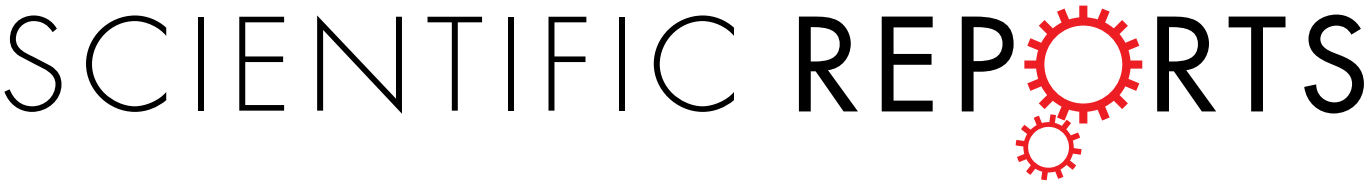

OPEN

Preparation and characterization of a new graphite superconductor: $Ca_{0.5}Sr_{0.5}C_6$

Received: 16 March 2017
Accepted: 29 June 2017
Published online: 07 August 2017

Saki Nishiyama[1], Hidenori Fujita[2], Masatoshi Hoshi[2], Xiao Miao[1], Takahiro Terao[1], Xiaofan Yang[1], Takafumi Miyazaki[3], Hidenori Goto[1], Tomoko Kagayama[2], Katsuya Shimizu[2], Hitoshi Yamaoka[4], Hirofumi Ishii[5], Yen-Fa Liao[5] & Yoshihiro Kubozono[1]

We have produced a superconducting binary-elements intercalated graphite, $Ca_xSr_{1-x}C_y$, with the intercalation of Sr and Ca in highly-oriented pyrolytic graphite; the superconducting transition temperature, T_c, was ~3 K. The superconducting $Ca_xSr_{1-x}C_y$ sample was fabricated with the nominal x value of 0.8, *i.e.*, $Ca_{0.8}Sr_{0.2}C_y$. Energy dispersive X-ray (EDX) spectroscopy provided the stoichiometry of $Ca_{0.5(2)}Sr_{0.5(2)}C_y$ for this sample, and the X-ray powder diffraction (XRD) pattern showed that $Ca_{0.5(2)}Sr_{0.5(2)}C_y$ took the SrC_6-type hexagonal-structure rather than CaC_6-type rhombohedral-structure. Consequently, the chemical formula of $Ca_xSr_{1-x}C_y$ sample could be expressed as '$Ca_{0.5(2)}Sr_{0.5(2)}C_6$'. The XRD pattern of $Ca_{0.5(2)}Sr_{0.5(2)}C_6$ was measured at 0–31 GPa, showing that the lattice shrank monotonically with increasing pressure up to 8.6 GPa, with the structural phase transition occurring above 8.6 GPa. The pressure dependence of T_c was determined from the DC magnetic susceptibility and resistance up to 15 GPa, which exhibited a positive pressure dependence of T_c up to 8.3 GPa, as in YbC_6, SrC_6, KC_8, CaC_6 and $Ca_{0.6}K_{0.4}C_8$. The further application of pressure caused the rapid decrease of T_c. In this study, the fabrication and superconducting properties of new binary-elements intercalated graphite, $Ca_xSr_{1-x}C_y$, are fully investigated, and suitable combinations of elements are suggested for binary-elements intercalated graphite.

Some graphite intercalation compounds show superconductivity, and have attracted serious attention because of their high superconducting transition temperatures (T_c's). The highest-onset superconducting transition temperature, T_c^{onset}, is currently 11.5 K at ambient pressure (0 GPa)[1,2] and 15.1 K at 7.5 GPa for CaC_6[3]. However, despite much effort to make new graphite superconductors, no graphite superconductors with higher T_c^{onset} values than 11.5 K have been synthesized. In fact, the T_c values of graphite superconductors prepared by the intercalation of alkali metal atoms thus far were 136 mK for KC_8[4,5] and 23 mK for RbC_8[4]. The graphite superconductors prepared by alkali earth or lanthanide atoms were SrC_6 ($T_c = 1.65$ K)[6], BaC_6 ($T_c = 65$ mK)[7] and YbC_6 ($T_c = 6.5$ K)[1]. Furthermore, binary-elements intercalated graphite was first achieved in $KHgC_8$ ($T_c = 1.9$ K)[8]. Subsequently, some binary-elements intercalated graphite superconductors were realized such as $RbHgC_8$ ($T_c = 1.44$ K)[9], $KTl_{1.5}C_4$ ($T_c = 2.7$ K)[10], $KTl_{1.5}C_8$ ($T_c = 2.5$ K)[10], $CsBi_{0.55}C_5$ ($T_c = 4.05$ K)[11], $Li_3Ca_2C_6$ ($T_c = 11.15$ K)[12]. Recently, our group succeeded in synthesis of $Ca_xK_{1-x}C_8$ (6.5 – 11.5 K) for $0.33 \leq x \leq 1$[13]. Thus, binary-element intercalation has provided a family of superconductive graphites.

A positive pressure dependence of T_c^{onset} was observed in CaC_6, and the maximum T_c^{onset} reached 15.1 K at 7.5 GPa[3]. At higher pressure, the T_c^{onset} suddenly dropped. Such a pressure dependence was also observed for other metal-intercalated graphite superconductors. The maximum T_c^{onset} values were 7.1 K at 1.8 GPa for YbC_6[14], 2 K at 1 GPa for SrC_6[6], and 1.7 K at 1.5 GPa for KC_8[15]. Such a pressure dependence is characteristic of graphite superconductors. The increase in T_c^{onset} for CaC_6 was assigned to the softening of the in-plane Ca-Ca phonon and the hardening of the Ca-C phonon[3,16]. Moreover, the rapid decrease in T_c is attributed to the order-disorder transition

[1]Research Institute for Interdisciplinary Science, Okayama University, Okayama, 700-8530, Japan. [2]Center for Science and Technology under Extreme Conditions, Graduate School of Engineering Science, Osaka University, Osaka, 560-8531, Japan. [3]Research Laboratory for Surface Science, Okayama University, Okayama, 700-8530, Japan. [4]RIKEN SPring-8 Center, RIKEN, 1-1-1 Kouto, Sayo, Hyogo, 679-5148, Japan. [5]National Synchrotron Radiation Research Center, Hsinchu, 30076, Taiwan. Correspondence and requests for materials should be addressed to Y.K. (email: kubozono@cc.okayama-u.ac.jp)

relating to a large softening of the lattice under pressure[17]. Similar behavior under pressure was also observed for binary-elements intercalated graphite $Ca_{0.6}K_{0.4}C_8$, showing a maximum T_c of 11.6 K at 3.3 GPa[13].

The mechanism of superconductivity has been extensively discussed based on the theoretical calculation[18,19]. Calandra and Mauri[18] suggested clearly that the supecondsuctivity in CaC_6 is due to an electron-phonon mechanism, and carriers are mostly electrons in the Ca Fermi surface which couples with in-plane Ca-Ca phonon and out-of plane C-C phonons. They suggested the importance of Ca Fermi surface (not π^* band of graphite) for the superconductivity. On the other hand, Yang *et al*. experimetally showed the opening of a superconducting gap in the π^* band of graphite[19], suggesting that the superconductivity cannot be assigned to only interlayer band but interaction of π^* and interlayer bands. Thus, the mechanism is still under debate. Furthermore, the superconductivity of metal-doped graphene has recently been pursued from theretical and experimental points of view[20–22]. The study on metal-doped graphene may lead to the elucidation of superconductivity in metal-intercalated graphite, since graphene is a thin limit of graphite.

The X-ray diffraction (XRD) patterns of $Ca_xK_{1-x}C_y$ ($x \neq 1$) suggested a KC_8-type structure[13] (face-centered orthorhombic, space group No. 70, *Fddd*)[23], rather than a CaC_6-type structure (rhombohedral, space group No. 166, $R\bar{3}m$)[2]. The former (KC_8 structure) shows 'AαAβAγAδ', where 'A' refers to the graphene sheet, and α, β, γ, and δ refer to the four sites occupied by the metal atoms. On the other hand, the latter (CaC_6-structure) shows 'AαAβAγ' in which metal occupies three different sites. The most interesting point is that in $Ca_xK_{1-x}C_y$ the T_c is much higher than that of KC_8 despite the KC_8-type structure.

In this study, we discovered a new binary-elements intercalated graphite superconductor through the intercalation of Ca and Sr. The T_c values of $Ca_xSr_{1-x}C_y$ with $x = 0.8$ or 0.9 were ~3 K in the metal-intercalation to highly-oriented pyrolytic graphite (HOPG). Energy dispersive X-ray (EDX) spectroscopy showed the chemical composition of the prepared $Ca_xSr_{1-x}C_y$. The XRD pattern of $Ca_xSr_{1-x}C_y$ showed that the crystal structure is SrC_6-type (hexagonal, space group No. 194, $P6_3/mmc$)[24]. Therefore, the $Ca_xSr_{1-x}C_y$ sample was finally expressed '$Ca_xSr_{1-x}C_6$'. The pressure dependence of the XRD pattern of $Ca_xSr_{1-x}C_6$ showed monotonic shrinkage of the lattice up to 20 GPa. The pressure dependence of T_c for $Ca_xSr_{1-x}C_6$ showed a positive pressure dependence at 0–8.3 GPa, and a sudden drop in T_c was observed with applied pressure above 8.3 GPa. The magnetic characteristics of the $R - T$ plot for $Ca_xSr_{1-x}C_6$ were also studied at 0.80, 4.3 and 8.5 GPa.

Results

Preparation and characterization of superconducting $Ca_xSr_{1-x}C_y$ sample through metal doping of HOPG. The temperature (T) dependence of magnetic susceptibility, M/H, ($M/H - T$ plot) measured in zero-field cooling (ZFC) mode in $Ca_xSr_{1-x}C_y$ ($x = 0.8$) prepared by the intercalation of Sr and Ca to HOPG, which is expressed '$Ca_{0.8}Sr_{0.2}C_y$', is shown in Fig. 1a; M and H refer to magnetization and applied magnetic field, respectively. The optical image of $Ca_{0.8}Sr_{0.2}C_y$ sample is shown in Fig. 2a, which was bright-gold colour.

A rapid drop in M/H is observed below ~3.0 K, and T_c is 3.2 K; how to determine T_c is shown in the inset of Fig. 1a. The T_c^{onset} is 4.0 K from the $M/H - T$ plot in ZFC mode. The $M/H - T$ plot in field-cooling (FC) mode is shown in Fig. 1a, and the T_c was also estimated to be 3.2 K. The shielding fraction was estimated to be 100% at 2 K from the $M/H - T$ plot in ZFC mode. Thus, the $Ca_{0.8}Sr_{0.2}C_y$ sample is quite simply a bulk superconductor. On the other hand, we prepared the SrC_6 sample by the intercalation of Sr in HOPG, which did not show superconductivity down to 2 K, as seen from Fig. 1b. As the T_c^{onset} of SrC_6 is 1.65 K, the absence of superconductivity is reasonable, suggesting that the $Ca_{0.8}Sr_{0.2}C_y$ sample is not SrC_6 but Ca/Sr co-doped graphite ($Ca_xSr_{1-x}C_y$).

In this study, we changed nominal x value from 0 to 0.9 in $Ca_xSr_{1-x}C_y$. For $Ca_xSr_{1-x}C_y$ at $x \geq 0.7$, the superconductivity was observed. The $Ca_xSr_{1-x}C_y$ sample with nominal x of 0.9, $Ca_{0.9}Sr_{0.1}C_y$, provided both phases of CaC_6 ($T_c \approx 11$ K) and $Ca_xSr_{1-x}C_y$ ($T_c \approx 4$ K), while that with nominal x of 0.7, $Ca_{0.7}Sr_{0.3}C_y$, showed smaller fraction of superconductivity ($T_c \approx 2.5$ K). For the $Ca_xSr_{1-x}C_y$ sample at nominal x of 0.9, we measured the EDX spectra at eight different positions, which showed three different stoichiometry, $Ca_{0.98(1)}Sr_{0.02(1)}C_y$ (four points), $Ca_{0.58(6)}Sr_{0.42(6)}C_y$ (three points) and $Ca_{0.35}Sr_{0.65}C_y$ (only one point), consistent with two superconducting phases ($T_c \approx 11$ K and $T_c \approx 4$ K) as described above; the $Ca_{0.35}Sr_{0.65}C_y$ is probably lower T_c than 4 K. Furthermore, for the $Ca_xSr_{1-x}C_y$ sample at nominal x of 0.7, the EDX spectra were measured at five different positions, showing a single phase, $Ca_{0.2(1)}Sr_{0.8(1)}C_y$. This result is consistent with the observation of a single phase exhibiting a small superconducting volume fraction ($T_c \approx 2.5$ K). Thus, owing to the observation of a very large shielding fraction ($T_c = 3.2$ K) as shown in Fig. 1a, we investigated the $Ca_xSr_{1-x}C_y$ sample prepared with nominal value of $x = 0.8$ throughout this study. Finally, we may stress the validity of stoichiometry determined from EDX, based on the consistency between the EDX results and magnetic properties of the $Ca_xSr_{1-x}C_y$ samples.

The $M - H$ plot of $Ca_{0.8}Sr_{0.2}C_y$ at 2 K is shown in Fig. 1c, which shows typical superconducting $M - H$ behaviour. The lower critical filed, H_{c1}, was determined to be 20 Oe (see inset of Fig. 1c). This H_{c1} is much smaller than 500 Oe (at 6 K) of CaC_6[2]. The $M/H - T$ plots at different H's are shown in Fig. 1d. The $H_{c2} - T$ plot obtained from $M/H - T$ plots (Fig. 1d) is shown in the inset of Fig. 1d, and the H_{c2} at 0 K, $H_{c2}(0)$, was determined to be 200 Oe from the $H_{c2} - T$ plot using the Werthamer-Helfand-Hochenberg (WHH) formula, $H_{c2}(0) = -0.693 T_c (dH_{c2}/dT)_{T=Tc}$, indicating that the London penetration depth (λ) and Ginzburg Landau coherent length (ξ_{GL}) are 215 and 130 nm, respectively. The H_{c2} value is much smaller than 7000 Oe of CaC_6[2]. Here, it should be noted that the H_{c2} predicted from the $M - H$ plot at 2 K (Fig. 1c) seems to be higher than 4000 Oe. This is probably due to the contribution from a CaC_6 phase, because this sample contains a trace of CaC_6, as seen from Fig. 1a. This scenario would be reasonable because the $H_{c2}(0)$ of CaC_6 is 7000 Oe[2].

The EDX of $Ca_{0.8}Sr_{0.2}C_y$ is presented in Fig. 2b, and shows peaks due to Sr, Ca, O and C atoms. The presence of O atoms must be due to the oxidation of $Ca_{0.8}Sr_{0.2}C_y$ because the sample used for the EDX spectrum was once treated under atmospheric conditions before the EDX measurement, *i.e*., the contamination of O originates from an extrinsic factor. Therefore, the EDX spectrum suggests that the chemical composition of the $Ca_{0.8}Sr_{0.2}C_y$ sample can be expressed '$Ca_xSr_{1-x}C_y$'; the contamination of Li could not be confirmed by the EDX spectrum because

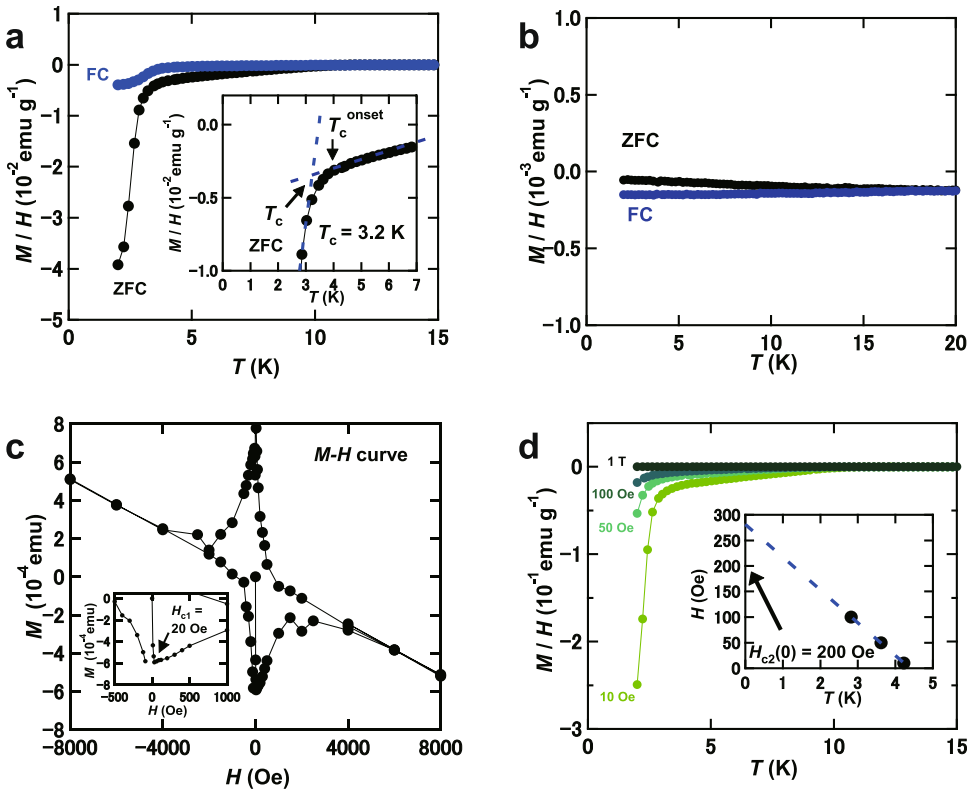

Figure 1. (**a**) $M/H - T$ plots in ZFC and FC modes for $Ca_{0.8}Sr_{0.2}C_y$. (**b**) $M/H - T$ plot in ZFC and FC modes for SrC_6. (**c**) $M - H$ plot at 2 K for $Ca_{0.8}Sr_{0.2}C_y$. (**d**) M/H - T plots at different H's for $Ca_{0.8}Sr_{0.2}C_y$, measured in ZFC mode. Inset of (**a**) shows how to determine the T_c. The inset of Fig. 1(c) shows the $M - H$ plot in the low-H range. Inset of (**d**): $H_{c2} - T$ plot for $Ca_{0.8}Sr_{0.2}C_y$ determined from (**d**). Stoichiometry of $Ca_{0.8}Sr_{0.2}C_y$ refers to the experimental nominal value, and all samples were made by the intercalation of Ca and Sr in HOPG.

the energy of the Li Kα peak is too low. The stoichiometry of $Ca_{0.8}Sr_{0.2}C_y$ was estimated to be $Ca_{0.5(2)}Sr_{0.5(2)}C_y$ from the area intensity of the peaks in the EDX spectrum. Here we can point out that since each peak is substantially resolved in the EDX spectrum (Fig. 2b), the area intensity is obtained with high accuracy. The estimated standard deviation (e.s.d.) of the chemical composition shown above was somewhat large when a large grain of $Ca_{0.8}Sr_{0.2}C_y$ was used for the EDX measurement, indicating that the sample was slightly inhomogeneous. From here, we use the chemical formula, $Ca_{0.5(2)}Sr_{0.5(2)}C_y$, for the $Ca_{0.8}Sr_{0.2}C_y$ sample.

Structure of superconducting $Ca_{0.5}Sr_{0.5}C_y$. The XRD pattern of $Ca_{0.5(2)}Sr_{0.5(2)}C_y$ at around 0 GPa is shown in Fig. 2c, indicating that the main peaks can be assigned to the SrC_6-type structure, which is $P6_3/mmc$ (No. 194)[24]. Simulation spectra (powder pattern) of LiC_6, CaC_6, SrC_6 and graphite are also shown in Fig. 2c; the simulation was made using the crystal structures of LiC_6[25], CaC_6[2] SrC_6[24], and graphite[26]. Furthermore, as seen from Fig. 2c, the relative intensity of the peaks observed is quite similar to that of SrC_6. Notably, the XRD pattern was measured with synchrotron radiation (wavelength $\lambda = 0.68841$ Å), in which the sample is introduced into a diamond anvil cell (DAC). The pressure was determined to be 0 GPa from the fluorescence of ruby, but the exact pressure may be 0–0.2 GPa.

The lattice constant, a, was determined to be 4.32 Å from the *100* and *110* peaks, while the lattice constant, c, was determined to be 9.82 Å from the *112* peak using the above a value. Furthermore, the values of a and c were evaluated using iterative approximation. In the iterative approximation, firstly we roughly estimated the a value from 100 and 110 peaks. Secondly, the c value was estimated from all peaks and the a value determined roughly in the first process. Finally the a value was estimated from the all peaks and the c determined in the second process. The a and c were 4.31(1) and 9.85(8) Å, respectively. The Le Bail fitting was also tried for determination of a and c. The a and c determined by Le Bail fitting were 4.3077(3) and 9.883(1) Å, respectively. Actually, because of the impurity peaks, the Le Bail fitting was difficult. Therefore, these values are for reference. The a and c values determined by all ways are consistent each other, implying that the a and c determined were reliable.

It is easy to assume that only 00l reflections will be measured, if the *ab*-plane of metal-intercalated HOPG sample is completely aligned to the sample holder. However, all reflections are observed as seen from indices of XRD pattern shown in Fig. 2c, indicating that the metal-intercalated HOPG sample is not completely aligned to the sample holder. Therefore, the XRD pattern observed is powder-like with preferred orientation. Consequently, we could successfully obtained both values of a and c. As seen from Fig. 2c, the XRD pattern of $Ca_{0.5}Sr_{0.5}C_y$ was simulated using $a = 4.31(1)$ and $c = 9.85(8)$ Å (iterative approximation) and assuming that the 50% of Ca and 50% of Sr randomly occupy the 2*c* site in the space group (No. 194, $P6_3/mmc$) of SrC_6-type crystal. As seen from

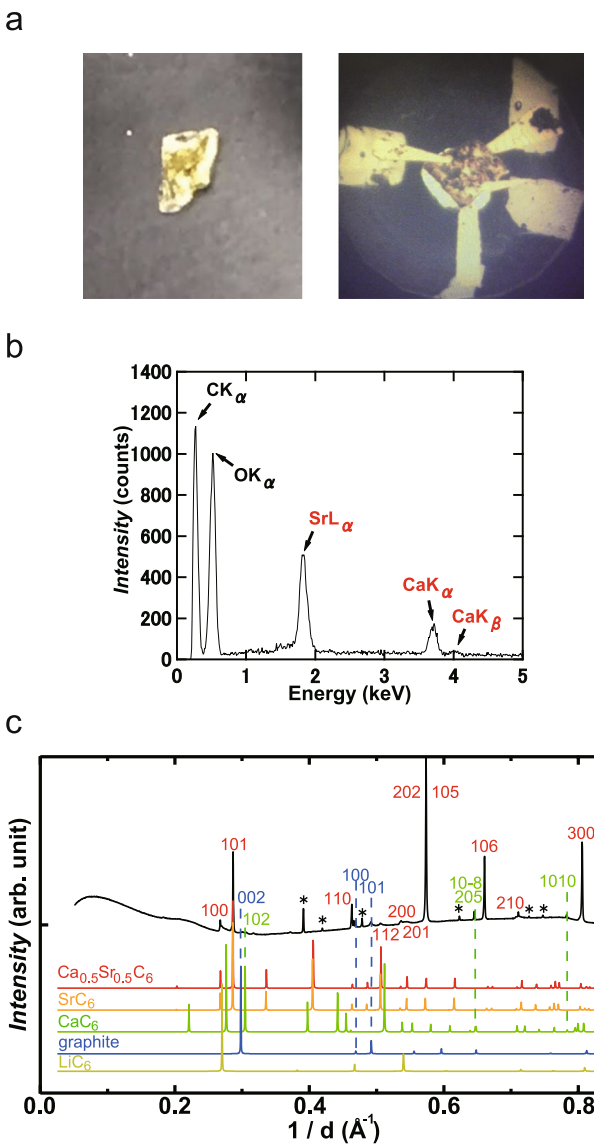

Figure 2. (**a**) Optical image (left) of the $Ca_{0.8}Sr_{0.2}C_y$ sample and microscope image (right) of the sample set in the DAC. (**b**) EDX spectrum of $Ca_{0.8}Sr_{0.2}C_y$. (**c**) XRD pattern of $Ca_{0.5(2)}Sr_{0.5(2)}C_y$. The XRD pattern was measured with synchrotron radiation of $\lambda = 0.68841$ Å at room temperature. Patterns shown in (**c**) for $Ca_{0.5}Sr_{0.5}C_6$, SrC_6, CaC_6, graphite and LiC_6 were simulated using the VESTA program, using structural data from refs 2, 24, 25 and 26, respectively.

the comparison between the experimenmtal XRD pattern and the simulated pattern of $Ca_{0.5}Sr_{0.5}C_6$ (Fig. 2c), most of peaks in the experimental XRD pattern for $Ca_{0.5(2)}Sr_{0.5(2)}C_y$ sample were assigned to those of $Ca_{0.5}Sr_{0.5}C_6$ simulated with SrC_6 structure. Thus, the indices for most of peaks were provided at SrC_6 structure, but some peaks were assigned to those of CaC_6 and graphite. Moreover, some of peaks were not assigned. The difference in relative intensities was found between the experimental XRD pattern and the simulated one of $Ca_{0.5}Sr_{0.5}C_6$, but the conclusion that the sample takes SrC_6 structure is supported. Furthermore, it should be noticed that to completely reproduce the relative intensities observed in the experimental XRD pattern is difficult, because it shows a powder-like pattern affected by strong preferred orientation, as described above.

The a and c values are almost the same as those ($a = 4.316$ Å and $c = 9.88$ Å) of SrC_6[24], and the simulated pattern of $Ca_{0.5}Sr_{0.5}C_y$ at SrC_6 structure is consistent with the experimental XRD pattern. As a results, all XRD results support that the stoichiometry of $Ca_{0.5(2)}Sr_{0.5(2)}C_y$ can be expressed '$Ca_{0.5(2)}Sr_{0.5(2)}C_6$'. The fact that the Ca/Sr binary-elements intercalated graphite takes the SrC_6 structure may be reasonable because the ionic radius of Sr^{2+} (1.18 Å for six coordination) is larger than that of Ca^{2+} (1.0 Å for six coordination). Namely, the Ca atoms may be intercalated into the crystal lattice of graphite separated by Sr atoms because of the larger ionic radius of Sr^{2+}. In this crystal, the metal atoms occupy two different sites of α and β, and the graphite layer shows AAA stacking. The stacking form, AαAβAα, of SrC_6 is different from that, AαAβAγAα, of CaC_6. The distance, d_{AA}, between graphenes in SrC_6 is 4.94 Å ($d_{AA} = c/2$), which is larger than the $d_{AA} = 4.524$ Å ($d_{AA} = c/3$) in CaC_6, indicating

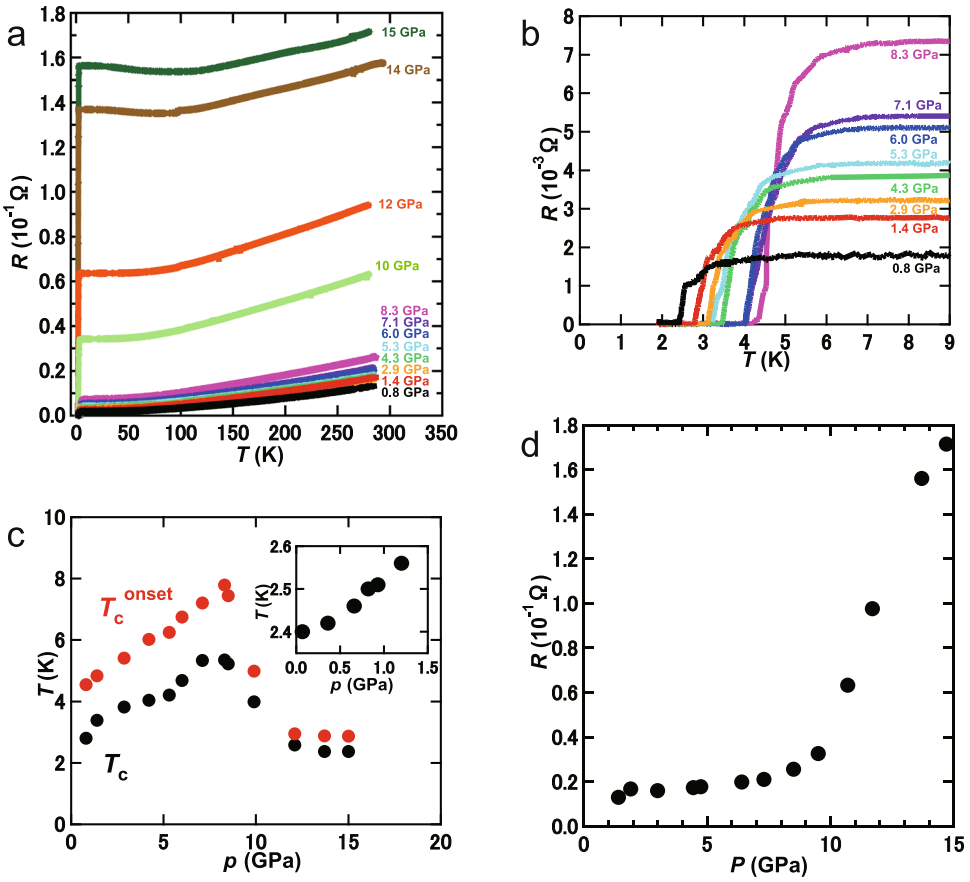

Figure 3. $R - T$ plots for $Ca_{0.5(2)}Sr_{0.5(2)}C_6$ at different pressures in T range of (**a**) 2–300 K and (**b**) 2–9 K. (c) $T_c - p$ and (**d**) $R - p$ plots for $Ca_{0.5(2)}Sr_{0.5(2)}C_6$; R in (**d**) means the R value at 280 K. Inset of (**c**): $T_c - p$ plot for the $Ca_{0.9}Sr_{0.1}C_y$ sample below 1.5 GPa, which was determined from $M/H - T$ plots at different pressures; this sample's stoichiometry is shown in the text.

that the Ca intercalation into SrC_6 (or $Ca_xSr_{1-x}C_y$) may not affect the lattice constant c. In fact, the c value of $Ca_{0.5(2)}Sr_{0.5(2)}C_6$ is almost the same as that of SrC_6, as described above. Thus, despite the SrC_6 structure, we could obtain the 3 K superconducting phase in $Ca_{0.5(2)}Sr_{0.5(2)}C_6$.

Finally, we must comment upon the peaks that cannot be assingned to $Ca_{0.5}Sr_{0.5}C_6$. Some of peaks were assigned to CaC_6 and pure graphite, as seen from Fig. 2c, indicating the presence of small amount of pure graphite in the sample. This may be the origin of the significant diamagnetic background observed in $M - H$ plot (Fig. 1c). As described previously, the presence of CaC_6 in the $Ca_{0.5(2)}Sr_{0.5(2)}C_6$ sample was suggested from the $M/H - T$ plot at ZFC mode shown in Fig. 1a. Here, it should be noticed that the $M/H - T$ at FC mode (Fig. 1a) did not show any trace of CaC_6. This may imply that the CaC_6 phase is not bulky but surface (thin layer). As seen from Fig. 2c, some of weak peaks in the XRD pattern were assigned to CaC_6, indicating the presence of CaC_6, which is consistent with the observation of a trace of CaC_6-superconductivity.

Pressure dependence of superconductivity and structure in $Ca_{0.5}Sr_{0.5}C_6$. Microscope image of $Ca_{0.5(2)}Sr_{0.5(2)}C_6$ sample and four electrodes set in DAC is shown in Fig. 2a, in which four electrodes are contacted to the sample. The sample shows bright-gold color. Figure 3a and b show the temperature dependence of resistance ($R - T$ plots) of $Ca_{0.5(2)}Sr_{0.5(2)}C_6$ at different pressures. The former shows the $R - T$ plots at 2–300 K, and the latter shows the expanded plots (2–9 K). The pressure dependence of T_c in $Ca_{0.5(2)}Sr_{0.5(2)}C_6$ is shown in Fig. 3c; the T_c was determined from the cross point of the $R - T$ plot at normal state and that exhibiting the drop, in the same manner as the inset of Fig. 1a. The T_c increased with increasing pressure up to 8.3 GPa, then suddenly decreased. This behaviour is similar to that of CaC_6[3] and $Ca_{0.6}K_{0.4}C_8$[13]. Such a positive pressure dependence of T_c in $Ca_{0.5(2)}Sr_{0.5(2)}C_6$ may also be due to the softening of in-plane Ca(Sr)-Ca(Sr) phonons, as suggested in CaC_6[3]. The highest T_c was 5.4 K at 8.3 GPa. The values of dT_c/dp and dT_c^{onset}/dp were determined to be 0.34(4) K GPa^{-1} and 0.42(1) K GPa^{-1}, respectively, from the $T_c - p$ and $T_c^{onset} - p$ plots at 0–8.3 GPa, consistent with those of SrC_6 and CaC_6 (dT_c/dp (SrC_6) = 0.35 K GPa^{-1} and dT_c^{onset}/dp (CaC_6) = 0.39 K GPa^{-1})[6,27]. The sudden drop of T_c is found in CaC_6 and $Ca_{0.6}K_{0.4}C_8$ which was assigned to the order-disorder transition originating from random off-center displacement of Ca(K) atoms in the *ab*-plane with accompanying lattice-softening[3,17]. Therefore, the T_c drop in the pressure range above 8.3 GPa for $Ca_{0.5(2)}Sr_{0.5(2)}C_6$ may be assigned to the above order-disorder transition.

The $R - T$ plots at H's of 0 and 500 Oe were measured at 0.80 GPa (Fig. 4a), indicating the suppression of superconductivity at 500 Oe. Furthermore, the $R - T$ plots at different H values were measured at 4.3 and 8.5 GPa.

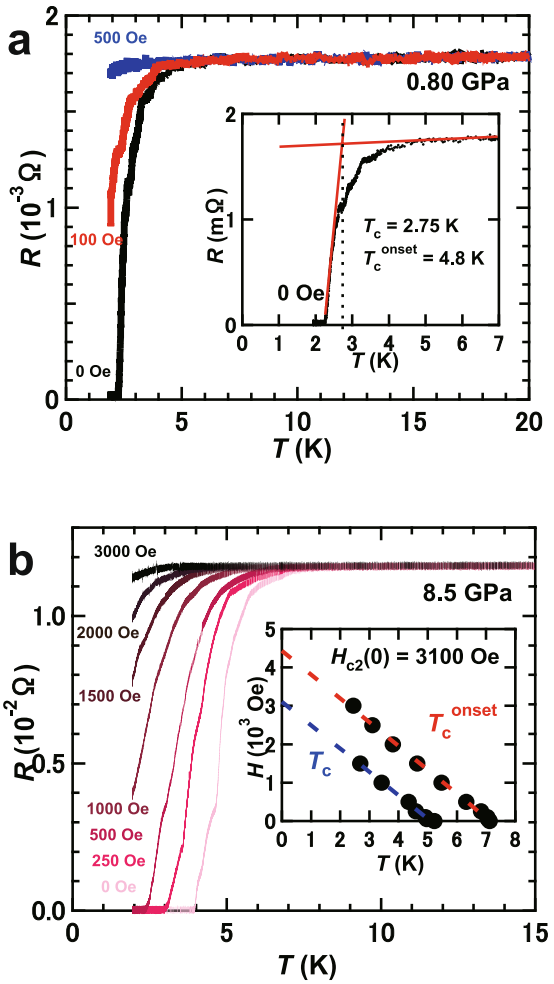

Figure 4. $R - T$ plots of $Ca_{0.5(2)}Sr_{0.5(2)}C_6$ at different H's under pressure of (**a**) 0.80 GPa and (**b**) 8.5 GPa. Inset of (**a**) shows how to determine T_c, and inset of (**b**) shows plots of $H - T_c^{onset}$ and $H - T_c$ for $Ca_{0.5(2)}Sr_{0.5(2)}C_6$. The $H - T_c^{onset}$ refers to $H_{c2} - T$ plot.

Figure 4b shows the $R - T$ plots at different H values at 8.5 GPa. The $H_{c2} - T$ plot determined from the graph shown in Fig. 4b is depicted in the inset of Fig. 4b. The $H_{C2}(0)$ at 8.5 GPa was evaluated to be 3100 Oe from the WHH formula. This value is larger than that, 200 Oe, evaluated from $M/H - T$ plots at 0 GPa (inset of Fig. 1d). Notably, as seen from Fig. 3a, the behavior of the $R - T$ plot in the normal state was metallic up to 12 GPa, *i.e.*, the R decreased with decreasing temperature. But at 14 and 15 GPa, the R increased slightly with decreasing temperature below 90 K, suggestive of a change in electric transport in the normal state at around 14 GPa (Fig. 3a). The $M/H - T$ plots at different pressures (0–1.3 GPa) for $Ca_{0.9}Sr_{0.1}C_y$ are shown in Fig. 1S of Supplementary Information, showing the positive pressure dependence. This sample contained three diffrenet phases, $Ca_{0.98(1)}Sr_{0.02(1)}C_y$, $Ca_{0.58(6)}Sr_{0.42(6)}C_y$ and $Ca_{0.35}Sr_{0.65}C_y$, as shown previously, but the stoichiometry exhibiting the T_c's determined from the $M/H - T$ plots (Figure S1) would be $Ca_{0.58(6)}Sr_{0.42(6)}C_y$ which is almost the same as $Ca_{0.5(2)}Sr_{0.5(2)}C_y$. The $T_c - p$ plot obtained from $M/H - T$ at 0–1.3 GPa is shown in the inset of Fig. 3c. Figure 3d shows the pressure dependence of R at 280 K for $Ca_{0.5(2)}Sr_{0.5(2)}C_6$. The R rapidly increases above 10 GPa, which may be correlated with the change in electric transport above 12 GPa shown in Fig. 3a.

Figure 5a–c show the pressure dependence of three representative peaks of $Ca_{0.5(2)}Sr_{0.5(2)}C_6$ in the XRD pattern. These peaks shifted to higher 2θ with an increase in pressure, indicating shrinkage of the unit cell. The *100* peak was observed up to 20 GPa, but suddenly disappeared above 20 GPa, while the *110* peak was clearly observed across the entire range of applied pressure (0–31 GPa). Moreover, the *112* peak quickly disappeared above 8.6 GPa. In $Ca_{0.6}K_{0.4}C_8$, the *004* peak completely disappeared at 16 GPa[13], which was assigned to the structural change from the KC_8 structure to a non-graphite type structure. The disappearance of the *112* peak at 10 GPa would be attributed to the vanishing of the long-range order of graphite, such as the graphite – non-graphite transition found at around 16 GPa in $Ca_{0.6}K_{0.4}C_8$[13]. Furthermore, the change of electric transport (Fig. 3a) and the rapid increase in R (Fig. 3d) may be explained by considering a structural transition at around 10 GPa.

The pressure dependence of lattice constants a and c is plotted in Fig. 5d and e; the a was determined up to 20 GPa, while c determined up to 8.6 GPa because of the rapid disappearance of the *112* peak around 10 GPa. Both plots show a monotonic shrinkage of the unit cell with increasing pressure. The pressure dependence of d_{AA} in

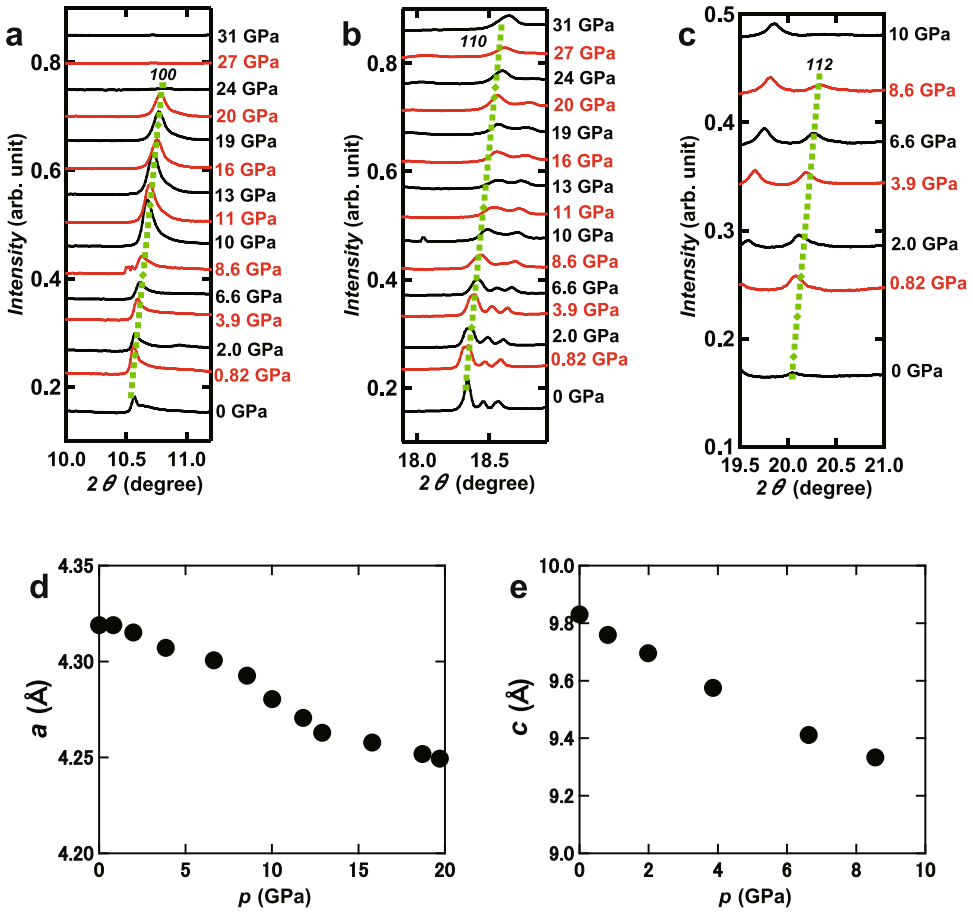

Figure 5. Pressure dependence of peaks ascribable to (**a**) *100*, (**b**) *110* and (**c**) *112* for $Ca_{0.5(2)}Sr_{0.5(2)}C_6$. (**d**) Pressure dependence of lattice constants, (**d**) *a* and (**e**) *c*, for $Ca_{0.5(2)}Sr_{0.5(2)}C_6$.

$Ca_{0.6}K_{0.4}C_8$ and $Ca_{0.5(2)}Sr_{0.5(2)}C_6$ is shown in Fig. 6; that of $Ca_{0.6}K_{0.4}C_8$ is taken from ref. 13. The behaviour of $d_{AA} - p$ is similar in both. Namely, the d_{AA} approaches the d_{AA} (=4.524 Å) of CaC_6 with increasing pressure, and any Bragg peak disappears when reaching that d_{AA} (above 13.7 GPa for $Ca_{0.6}K_{0.4}C_8$ and above 8.6 GPa for $Ca_{0.5(2)}Sr_{0.5(2)}C_6$). To sum up, any structural transition may take place when the d_{AA} reaches the threshold value of d_{AA}.

Discussion

In this paper, the most important issue is that a new class of superconducting binary-elements intercalated graphite was prepared by the intercalation of Sr and Ca. These are alkali-earth elements, and their ionic radii differ slightly (Sr^{2+}: 1.18 Å for six coordination and Ca^{2+}: 1.0 Å for six coordination). The ionic radii of some elements which can be intercalated to graphite are shown in Table 1, in which they were taken form ref. 28. On the other hand, the crystal structure is different between CaC_6 and SrC_6, in which the former takes the rhombohedral structure (space group No. 166, $R\bar{3}m$)[2], while the latter takes the hexagonal structure (space group No. 194, $P6_3/mmc$)[24]. In both crystals, the graphene sheets stack in AAA form, but location of Ca or Sr is different; AαAβAγA for CaC_6, and AαAβA for SrC_6. Previously, we successfully made the superconducting $Ca_xK_{1-x}C_y$ materials which consist of alkali and alkali earth elements. The ionic radii of Ca and K are 1.0 Å (for six coordination) and 1.38 Å (for six coordination), respectively, which are quite different. The crystal of KC_8 takes face-centered orthorhombic structure (space group No. 70, *Fddd*), in which the stacking form is AαAβAγAδA, different from that of CaC_6. Regardless of such a large difference between CaC_6 and KC_8, $Ca_xK_{1-x}C_y$ was successfully formed.

On the other hand, we tried to fabricate $Ca_xYb_{1-x}C_y$, but the $M/H - T$ plot showed a complete phase separation of CaC_6 (T_c = 11.5 K) and YbC_6 (T_c = 6.7 K), as seen from Fig. 7. The crystal structure of YbC_6 is the same as that of SrC_6. The ionic radius of Yb is 1.02 Å for six coordination, which is the same as that of Ca. Nevertheless, the $Ca_xYb_{1-x}C_y$ could not be realized thus far. The liquid alloy method has been used for the preparation of binary-elements intercalated graphites, and the YbC_6 and CaC_6 phases were separately generated in the preparation of $Ca_xYb_{1-x}C_y$, suggesting both elements are melted. Therefore, we can rule out the possibility of no melting of either element.

Here, we focus on the fact that the element with the larger ionic radius dominates the crystal structure, *i.e.*, the SrC_6 structure in $Ca_xSr_{1-x}C_y$ and the KC_8 structure in $Ca_xK_{1-x}C_y$. Furthermore, the d_{AA} in binary-elements intercalated graphite is the same as that of a crystal lattice consisting solely of an element with larger ionic radius; the d_{AA} (=c /2 = 4.91 Å (c = 9.81 Å) or 4.925 Å (c = 9.85(8) Å) of $Ca_xSr_{1-x}C_y$ is the same as that (=c/2 = 4.95 Å) of SrC_6, and the d_{AA} = (c /4 = 5.40 Å) of $Ca_xK_{1-x}C_8$ is the same as that (=c/4 = 5.35 Å)[23] of KC_8, as seen from Fig. 2

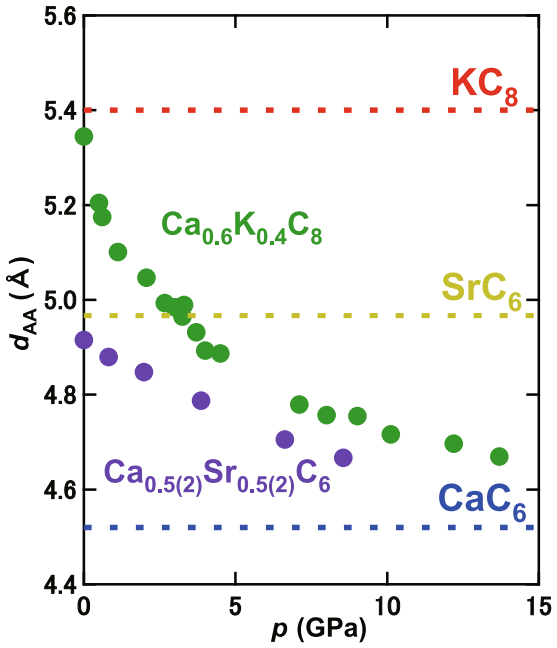

Figure 6. Pressure dependence of d_{AA} for $Ca_{0.6}K_{0.4}C_8$ and $Ca_{0.5(2)}Sr_{0.5(2)}C_6$. Dashed lines drawn in red, yellow and blue refer to the d_{AA} values of KC_8, SrC_6 and CaC_6, respectively.

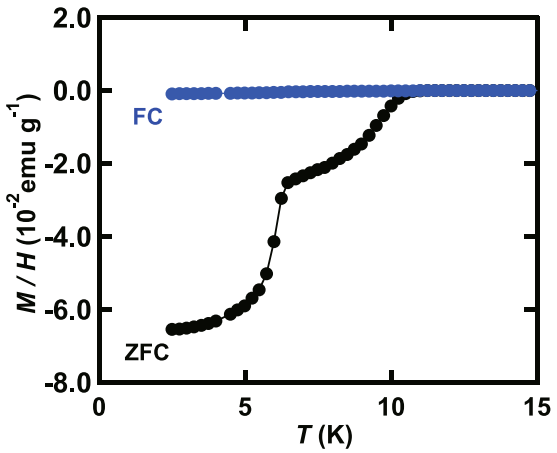

Figure 7. $M/H - T$ plots in ZFC and FC modes for $Ca_{0.8}Yb_{0.2}C_y$. Presence of two phases of CaC_6 and YbC_6 is indicated.

Element	Coordination number	Ionic radius (Å)
Li	6	0.76
K	6	1.38
Cs	6	1.67
Ca	6	1.0
Sr	6	1.18
Yb	6	1.02

Table 1. Ionic radius of elements (from ref. 28).

of ref. 23. These facts may point to a scenario in which the crystal lattice formed by the element with larger ionic radius is subsequently doped with the other element with smaller ionic radius. Based on this scenario, we can propose suitable combinations for the superconducting binary-elements or ternary-elements intercalated graphites, *i.e.*, the binary-elements graphites must be realized using Cs and Ca, or Cs and Yb, because of the larger difference

in ionic radii (Cs^+: 1.67 Å for six coordination), and for the ternary-elements superconductors the combination of Ca (or Yb), Sr (or K) and Cs are probably suitable. The crystal structure of the binary- and ternary-elements intercalated graphites suggested above would be the CsC_8-type structure, because the CsC_8 phase is formed with the CsC_8 structure[29].

Methods

Sample preparation and characterization. The $Ca_xSr_{1-x}C_y$ samples were prepared using the liquid-alloy method. Ca and Sr metals were mixed in appropriate molar ratios and placed in an iron vessel with Li. The molar ratio of Li was the same as the sum of Ca and Sr. The vessel was then heated to 350 °C, at which temperature the Ca/Sr/Li alloy was completely melted. The HOPG was immersed in the molten Ca/Sr/Li alloy for approximately one week. The whole preparation was performed in an Ar-filled glove box (O_2 and H_2O concentrations were maintained below 0.1 ppm). The $M/H - T$ curves of the $Ca_xSr_{1-x}C_y$ samples were measured with a SQUID magnetometer (Quantum Design, MPMS2). All XRD patterns at 0–31 GPa were measured at 295 K using synchrotron radiation ($\lambda = 0.68841$ Å) at BL12B2 of SPring-8. The simulated XRD patterns for LiC_6, CaC_6 and SrC_6 made using the VESTA program[30] were employed for the analyses of XRD patterns.

The diamond anvil cell was used for the measurements, and the $Ca_{0.5(2)}Sr_{0.5(2)}C_6$ sample was placed in the diamond anvil cell without any exposure of the sample to air, as is described below. A 300-μm-thick stainless steel gasket with a 160-μm diameter hole was placed on a diamond with a 400-μm culet, and the sample was introduced into the hole. The sample was covered with daphne oil (Idemitsu Co., Ltd., Daphne 7373) as the pressure medium. Finally the sample was pressed by another diamond. The pressure was monitored by the fluorescence peak of a piece of ruby set in the DAC. The pressure dependence of the $M/H - T$ plot for $Ca_xSr_{1-x}C_y$ was measured using the above SQUID equipment in which the sample was placed in a piston-cylinder cell; the pressure medium was the same daphne oil as above. Meanwhile, the pressure dependence of the $R - T$ plots was measured in four-terminal measurement mode; the used sample was identified to be $Ca_{0.5(2)}Sr_{0.5(2)}C_6$. The sample was placed in a diamond anvil cell (DAC); the pressure medium was NaCl. Details of sample-setting for the $M/H - T$ and $R - T$ measurements at high pressure are described elsewhere[13]. The R was recorded using an AC resistance-bridge (Lakeshore, 370-type Resistance Bridge), limiting the applied current to less than 100 μA. The sample was cooled using liquid He, and the temperature was controlled with a temperature controller (Oxford, ITC503 Temperature Controller).

References

1. Weller, T. E., Ellerby, M., Saxena, S. S., Smith, R. P. & Skipper, N. T. Superconductivity in the intercalated graphite compounds C_6Yb and C_6Ca. *Nat. Phys.* **1**, 39–41 (2005).
2. Emery, N. *et al*. Superconductivity of bulk CaC_6. *Phys. Rev. Lett.* **95**, 087003 (2005).
3. Gauzzi, A. *et al*. Enhancement of superconductivity and evidence of structural instability in intercalated graphite CaC_6 under high pressure. *Phys. Rev. Lett.* **98**, 067002 (2007).
4. Hannay, N. B. *et al*. Superconductivity in graphitic compounds. *Phys. Rev. Lett.* **14**, 225–226 (1965).
5. Koike, Y., Suematsu, H., Higuchi, K. & Tanuma, S. Superconductivity in graphite-alkali metal intercalation compounds. *Physica* 99B, (503–508 (1980).
6. Kim, J. S., Boeri, L., O'Brien, J. R., Razavi, F. S. & Kremer, R. K. Superconductivity in heavy alkaline-earth intercalated graphites. *Phys. Rev. Lett.* **99**, 027001 (2007).
7. Heguri, S. *et al*. Superconductivity in the graphite intercalation compound BaC_6. *Phys. Rev. Lett.* **114**, 247201 (2015).
8. Alexander, M. G. & Goshorn, D. P. Synthesis and low temperature specific heat of the graphite intercalation compounds $KHgC_4$ and $KHgC_8$. *Synth. Met.* **2**, 203–211 (1980).
9. Pendrys, L. A. *et al*. Superconductivity of the graphite intercalation compounds $KHgC_8$ and $RbHgC_8$. *Solid. State. Commun.* **38**, 677–681 (1981).
10. Wachnik, R. A., Pendrys, L. A., Vogel, F. L. & Lagrange, P. Superconductivity of graphite intercalated with thallium alloys. *Solid. State. Commun.* **43**, 5–8 (1982).
11. Lagrange, P., Bendriss-Rerhrhaye, A., Mareche, J. F. & Mcrae, E. Systhesis and electrical properties of some new ternary graphite intercalation compounds. *Synth. Met.* **12**, 201–206 (1985).
12. Emery, N. *et al*. Superconductivity in $Li_3Ca_2C_6$ intercalated graphite. *J. Solid. State. Chem.* **179**, 1289–1292 (2006).
13. Nguyen, H. T. L. *et al*. Fabrication of new superconducting materials, $Ca_xK_{1-x}C_y$ ($0 < x < 1$). *Carbon* **100**, 641–646 (2016).
14. Akrap, A. *et al*. C_6Yb and graphite: A comparative high-pressure transport study. *Phys. Rev. B* **76**, 045426 (2007).
15. Delong, L. E. *et al*. Observation of anomalies in the pressure dependence of the superconducting transition temperature of potassium-based graphite intercalation compounds. *Phys. Rev. B* **26**, 6315–6318 (1982).
16. Kim, J. S., Boeri, L., Kremer, R. K. & Razavi, F. S. Effect of pressure on superconducting Ca-intercalated graphite CaC_6. *Phys. Rev. B* **74**, 214513 (2006).
17. Gauzzi, A. *et al*. Maximum T_c at the verge of a simultaneous order-disorder and lattice-softening transition in superconducting CaC_6. *Phys. Rev. B* **78**, 064506 (2008).
18. Calandra, M. & Mauri, F. Theoretical explanation of superconductivity in C_6Ca. *Phys. Rev. Lett.* **95**, 237002 (2005).
19. Yang, S.-L. *et al*. Superconducting graphene sheets in CaC6 enlabled by phonon-mediated interband interactions. *Nat. Commun.* **5**, 3493 (2014).
20. Rahnejat, K. C. *et al*. Charge density waves in the graphene sheets of the superconductor CaC_6. *Nat. Commun.* **2**, 558 (2011).
21. Profeta, G., Calandra, M. & Mauri, F. Phonon-mediated superconductivity in graphene by lithium deposition. *Nat. Phys.* **8**, 131–134 (2012).
22. Chapman, J. *et al*. Superconductivity in Ca-doped graphene laminates. *Sci. Rep.* **6**, 23254 (2016).
23. Hérold, A., Billaud, D., Guérard, D., Lagrange, P. & Makrini, M. E. Intercalation of metals and alloys into graphite. *Physica B* **105**, 253–260 (1981).
24. Guérard, D. & Hérold, A. Chimie Macromoléculaire. Synthèse directe de composés d'insertion du strontium dans le graphite. *C. R. Seances Acad. Sci. C* **280**, 729–730 (1975).
25. Kganyago, K. R. & Ngoepe, P. E. Structural and electronic properties of lithium intercalated graphite LiC_6. *Phys. Rev. B* **68**, 205111 (2003).
26. Zhao, Y.-X. & Spain, I. L. X-ray diffraction data for graphite to 20 GPa. *Phys. Rev B* **40**, 993–987 (1989).
27. Debessai, M. *et al*. Superconductivity for CaC_6 to 32 GPa hydrostatic pressure. *Phys. Rev. B* **82**, 132502 (2010).
28. Shannon, R. D. Revised effective ionic radii and systematic studies of interatomic distances in halides and chalcogenides. *Acta Cryst. A* **32**, 751–767 (1976).

29. Guerard, D., Lagrange, P., Mohamed, E. M. & Hérold, A. Etude structurale du graphiture I de cesium. *Carbon* **16**, 285–290 (1978).
30. Momma, K. & Izumi, F. An integrated three-dimensional visualization system VESTA using wxWidgets. *Commission on Crystallogr. Comput.* **7**, 106–119 (2006).

Acknowledgements

This study was partly supported by Grants-in-aid (26105004, 26400361 and 15K05477) from MEXT and by the Program for Promoting the Enhancement of Research Universities. This work was partly supported by JST ACT-C Grant Number JPMJCR12YW, Japan. The XRD measurements were performed at the proposal of 2016B4131 of SPring-8.

Author Contributions

Y.K. suggested the idea for this research, and designed this study with S.N., who prepared and characterised all of the $Ca_xSr_{1-x}C_y$ samples with the assistance of X.M. and T.T. The X-ray diffraction of the sample was measured at BL12B2 of SPring-8 by T.T., H.Y., H.I., Y.-F.L. and Y.K; the diamond anvil cell used for pressure-dependent X-ray diffraction was designed by H.Y. The pressure-dependent $M/H - T$ measurement was done by S.N. and T.M. EDX measurement was done by S.N. and X.Y. Pressure-dependent $R - T$ measurement was made by H.F., M.H., K.S., T.K. and S.N.; the experimental setup for $R - T$ measurement was designed by K.S. and T.K. All data were analysed by S.N., T.T. and X.Y. under continuous discussion with Y.K. and H.G. The manuscript was prepared by Y.K. with discussions with all authors.

Additional Information

Supplementary information accompanies this paper at doi:10.1038/s41598-017-07763-y

Competing Interests: The authors declare that they have no competing interests.

Publisher's note: Springer Nature remains neutral with regard to jurisdictional claims in published maps and institutional affiliations.